

Article

Evaluation and Projection of Near-Surface Wind Speed over China Based on CMIP6 Models

Hao Deng ¹, Wei Hua ^{1,2,3,*}  and Guangzhou Fan ²

¹ School of Atmospheric Science, Chengdu University of Information Technology, Chengdu 610225, China; 3190101037@cuit.edu.cn

² Plateau Atmosphere and Environment Key Laboratory of Sichuan Province, Chengdu 610225, China; fgz@cuit.edu.cn

³ Meteorological Disaster Prediction and Warning Engineering Laboratory of Sichuan Province, Chengdu 610225, China

* Correspondence: huawei@cuit.edu.cn

Abstract: The characteristics of near-surface wind speed (NWS) are important to the study of dust storms, evapotranspiration, heavy rainfall, air pollution, and wind energy development. This study evaluated the performance of 30 models of the Coupled Model Intercomparison Project Phase 6 (CMIP6) through comparison with observational NWS data acquired in China during a historical period (1975–2014), and projected future changes in NWS under three scenarios (SSP1-2.6, SSP2-4.5, and SSP5-8.5) based on an optimal multi-model ensemble. Results showed that most models reproduced the spatial pattern of NWS for all seasons and the annual mean, although the models generally overestimated NWS magnitude. All models tended to underestimate the trends of decline of NWS for all seasons and the annual mean. On the basis of a comprehensive ranking index, the KIOST-ESM, CNRM-ESM2-1, HadGEM3-GC31-LL, CMCC-CM2-SR5, and KACE-1-0-G models were ranked as the five best-performing models. In the projections of future change, nationally averaged NWS for all months was weaker than in the historical period, and the trends decreased markedly under all the different scenarios except the winter time series under SSP2-4.5. Additionally, the projected NWS over most regions of China weakened in both the early period (2021–2060) and the later period (2061–2100).

Keywords: CMIP6; near-surface wind speed; China; evaluation; projection



Citation: Deng, H.; Hua, W.; Fan, G. Evaluation and Projection of Near-Surface Wind Speed over China Based on CMIP6 Models. *Atmosphere* **2021**, *12*, 1062. <https://doi.org/10.3390/atmos12081062>

Academic Editors: Bo Sun and Helene R. Langehaug

Received: 14 July 2021

Accepted: 12 August 2021

Published: 18 August 2021

Publisher's Note: MDPI stays neutral with regard to jurisdictional claims in published maps and institutional affiliations.



Copyright: © 2021 by the authors. Licensee MDPI, Basel, Switzerland. This article is an open access article distributed under the terms and conditions of the Creative Commons Attribution (CC BY) license (<https://creativecommons.org/licenses/by/4.0/>).

1. Introduction

The development of wind energy over recent decades is unprecedented. Wind energy, which is the renewable energy source being developed most rapidly globally, is recognized as the most cost-effective carbon emission control technology in relation to carbon-neutral and renewable sources of electricity. In 2020, global wind energy had reached 744 GW (289 GW in China) of total installed capacity, supplying more than 7% of global energy [1]. The near-surface wind speed (NWS) is a critical index with which to quantify wind resource potential. However, climate change can directly influence the spatiotemporal distribution and quality (or output) of wind energy [2,3]. Furthermore, changes in NWS associated with the increasing frequency and intensity of extreme weather events, resulting from climate change, could be detrimental to the operation of wind farms and cause uncertainty regarding the use of renewable energy sources [4–6].

In China, observed NWS has decreased consistently over recent decades but with strong regional and seasonal differences. For example, Wang et al. [7] examined the change in wind speed during 1951–2000 and found significant weakening, especially in northwest China during winter. Niu et al. [8] found that spatially averaged NWS has dropped from 3.7 to 3.0 m·s⁻¹. Guo et al. [9] showed that the average rate of decrease in annual mean wind speed over China has reached $-0.018 \text{ m}\cdot\text{s}^{-1} \text{ a}^{-1}$, with the largest rate of decline in

spring ($-0.021 \text{ m}\cdot\text{s}^{-1}\cdot\text{a}^{-1}$) and the smallest rate of decline in summer ($-0.015 \text{ m}\cdot\text{s}^{-1}\cdot\text{a}^{-1}$). The causes of the decline in NWS over recent decades in China have yet to be conclusively identified. You et al. [10] reported that the annual and seasonal mean wind speeds over the Tibetan Plateau (TP) during 1980–2005 diminished statistically, and that weakened latitudinal gradients of both regional temperature and surface pressure caused by TP warming may account, in part, for the observed decline in wind speed. Additionally, Wu et al. [11] revealed that changes in land use and land cover have had significant impacts on NWS over the East China Plain.

Changes in NWS could occur in future decades because of ongoing climate change. The Coupled Model Intercomparison Project (CMIP) organized by the World Climate Research Program has provided new scientific data from global climate models (GCMs) to enable study of the effects of different emission scenarios on future climate change. Model data from Phases 3 and 5 of CMIP (CMIP3 and CMIP5) have been used widely in NWS research. For example, using a multi-model database from CMIP3, Rahim et al. [12] analyzed the effects of global warming on the average wind speed field in central Japan in the 21st century. Mohan and Bhaskaran [13] evaluated CMIP5 climate model projections of NWS over the Indian Ocean region. Future changes in NWS over China have also been investigated. For example, Jiang et al. [14,15] applied CMIP3 and CMIP5 databases to validation and projection of future NWS over China, and they found that CMIP3 and CMIP5 GCMs could realistically capture the spatial patterns of annual and seasonal mean wind speed, but that they tended to underestimate the trends of decline. Abolude et al. [16] assessed the potential status of future wind power over China using CMIP5 models. Zha et al. [17] projected future changes in NWS over eastern China based on 24 CMIP5 GCMs under two representative concentration pathway scenarios (i.e., RCP4.5 and RCP8.5).

Recently, CMIP Phase 6 (CMIP6) was launched to address scientific questions in the field of climate studies [18]. In comparison with CMIP5, the most notable difference in CMIP6 is that the models consider both RCPs and Shared Socioeconomic Pathways (SSPs) [19]. With increasing availability of state-of-the-art GCMs, many studies have investigated the future climate of China, including the mean climate and climatic extremes such as droughts and floods [20–22]. However, few studies have evaluated the performance of CMIP6 models in simulating NWS in China. Therefore, this study evaluated and projected changes in NWS over China using CMIP6 GCMs.

The remainder of this paper is organized as follows. Section 2 presents the data and methods used. In Section 3, the performance of the CMIP6 GCMs is discussed, and Section 4 analyzes the future changes in NWS over China. Finally, Section 5 presents a discussion and the derived conclusions.

2. Data and Methods

2.1. Observations and CMIP6 Simulations

Two datasets were used in this study. The first comprised monthly NWS data (1975–2014) recorded at 2272 national meteorological stations that were provided by the China meteorological data service centre. The distribution of the locations of the meteorological stations is shown in Figure 1.

The second dataset consisted of outputs from 30 CMIP6 GCMs (<https://esgf-node.llnl.gov/projects/cmip6/>, accessed on 11 August 2021). Brief information regarding the name and horizontal resolution of each GCM together with details of the relevant institution and country are listed in Table 1. For evaluation purposes, this study focused on the period 1975–2014 (hereafter, called the historical period). Additionally, future projections of NWS in China were generated under three SSPs (i.e., SSP1-2.6, SSP2-4.5, and SSP5-8.5, which represent low-, moderate-, and high-emission scenarios, respectively). Here, only the first realization, first initialization, and first physics (r1i1p1) for each model were considered, based on data availability at the time of undertaking this study. To unify the resolution of the observational data and model outputs, all data were interpolated to $1^\circ \times 1^\circ$ resolution per grid for NWS over mainland China ($17\text{--}55^\circ \text{ N}$, $72\text{--}138^\circ \text{ E}$), using

the bilinear interpolation approach (CMIP6 data) or the Gressman interpolation approach (station data).

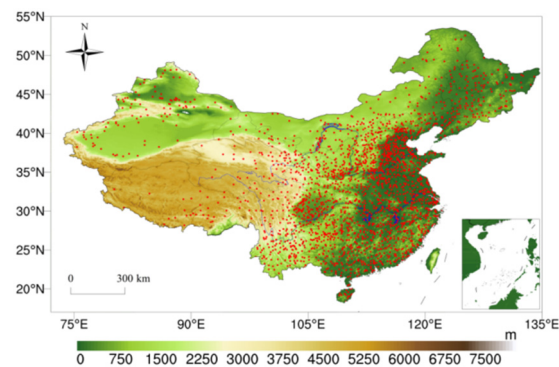


Figure 1. Generalized topography of China and distribution of the national meteorological stations considered in this study.

Table 1. Information regarding the CMIP6 models' name, institute/country, and horizontal resolution used in this study, where lat (lon) meaning latitude (longitude).

Model	Institute/Country	Horizontal Resolution (lat × lon)
ACCESS-CM2	CSIRO-ARCCSS/Australia	144 × 192
ACCESS-ESM1-5	CSIRO/Australia	145 × 192
AWI-CM-1-1-MR	AWI/Germany	192 × 384
BCC-CSM2-MR	BCC/China	160 × 320
CAMS-CSM1-0	CAMS/China	160 × 320
CanESM5	CCCma/Canada	64 × 128
CESM2-WACCM	NCAR/USA	192 × 288
CMCC-CM2-SR5	CMCC/Italy	192 × 288
CNRM-CM6-1	CNRM-CERFACS/France	128 × 256
CNRM-CM6-1-HR		360 × 720
CNRM-ESM2-1		128 × 256
EC-Earth3	EC-Earth-Consortium/Europe	256 × 512
EC-Earth3-Veg		256 × 512
FGOALS-f3-L	IAP/China	180 × 288
FGOALS-g3		80 × 180
GISS-E2-1-G	NASA-GISS/USA	90 × 144
HadGEM3-GC31-LL	MOHC/UK	144 × 192
INM-CM4-8	INM/Russia	120 × 180
INM-CM5-0		
IPSL-CM6A-LR	IPSL/France	144 × 143
KACE-1-0-G	KMA/Korea	144 × 192
KIOST-ESM	KIOST/Korea	96 × 192
MIROC6	MIROC/Japan	128 × 256
MIROC-ES2L		64 × 128

Table 1. *Cont.*

Model	Institute/Country	Horizontal Resolution (lat × lon)
MPI-ESM1-2-HR MPI-ESM1-2-LR	MPI-M/Germany	192 × 384 96 × 192
MRI-ESM2-0	MRI/Japan	160 × 320
NorESM2-LM NorESM2-MM	NCC/Norway	96 × 144 192 × 288
UKESM1-0-LL	MOHC/UK	144 × 192

2.2. Methodology

To compare the simulation performance of the CMIP6 GCMs in terms of the spatial features and interannual variability of NWS over China, this study used Taylor diagrams [23], relative bias (*BIAS*), the interannual variability score (*IVS*), and the comprehensive ranking (*MR*) index.

The spatial correlation coefficient (*R*), root mean square error (*RMSE*), standard deviation of the simulated field (σ_M), and standard deviation of the observation field (σ_O) are used most often to quantify similarities between the spatial patterns of modeled and observational data. The Taylor diagram, which is used widely in the evaluation of climate models, provides a visual framework for displaying four statistics in a single interpreted diagram. The specific formulas for calculating the statistics can be expressed as follows:

$$\sigma_M = \sqrt{\frac{1}{n} \sum_{i=1}^n (M_i - \bar{M})^2} \tag{1}$$

$$\sigma_O = \sqrt{\frac{1}{n} \sum_{i=1}^n (O_i - \bar{O})^2} \tag{2}$$

$$R = \frac{\frac{1}{n} \sum_{i=1}^n (M_i - \bar{M})(O_i - \bar{O})}{\sigma_M \sigma_O} \tag{3}$$

$$RMSE = \sqrt{\frac{1}{n} \sum_{i=1}^n [(M_i - \bar{M}) - (O_i - \bar{O})]^2} \tag{4}$$

where i , M_i , O_i , \bar{M} , and \bar{O} represent the number of grid points distributed over China in this study, the simulated value, the observed value, the average value of the simulation, and the average value of the observation, respectively. The four statistics satisfy the following relationship in the Taylor diagram:

$$RMSE^2 = \sigma_M^2 + \sigma_O^2 - 2\sigma_M\sigma_O R \tag{5}$$

The Taylor diagram evaluates the similarity of normalized fields and therefore σ_M is equal to 1. An additional deviation statistic can be added to the evaluation of spatial features, which is calculated as follows:

$$BIAS = \frac{\frac{1}{n} \sum_{i=1}^n (M_i - O_i)}{\frac{1}{n} \sum_{i=1}^n O_i} \times 100\% \tag{6}$$

In addition to spatial features, temporal variation is another fundamental factor in validation of model performance. As in Chen et al. [24], the *IVS* can be defined as follows:

$$IVS = \left(\frac{STD_M}{STD_O} - \frac{STD_O}{STD_M} \right)^2 \quad (7)$$

where STD_M and STD_O represent the interannual standard deviation of the simulation and observation, respectively. This statistic is symmetrical, that is, when the interannual variability of the simulation is half that of the observation, the calculated value is equal to that when the interannual variability is twice that of the observation. This represents one of the main advantages of this statistical variable because underestimation of the interannual variability of the observation is more detrimental than its overestimation [25]. Equation (7) shows that the *IVS* value is equal to 0 when STD_M is equivalent to STD_O ; thus, the closer the *IVS* value is to 0, the better the capability of simulating interannual variation.

The simulation performance of climate models varies seasonally and annually. Similar to Jiang et al. [26], this study used the *MR* index for comprehensive evaluation of model performance:

$$MR = 1 - \frac{1}{nm} \sum_{i=1}^n Rank_i \quad (8)$$

where m , n , and $Rank_i$ represent the number of models, the statistics, and the relative ranking of the corresponding model of different evaluation indices, respectively. Therefore, in the analysis in this paper, m is 30, and because the normalized *RMSE* of the Taylor diagram can represent the spatial correlation coefficient and the standard deviation according to Equation (5), n is 15, which represents the normalized *RMSE*, *BIAS*, and *IVS* of each season and annually, respectively. The value of *MR* is closest to 1 (0) when the ranking of all statistics for a given model is 1 (30).

3. Model Evaluation

3.1. Climatology

To quantitatively evaluate the simulation performance of the CMIP6 GCMs in reproducing the spatial pattern of seasonal (March–May, MAM; June–August, JJA; September–November, SON; December–February, DJF) and annual mean NWS over China, the climatological patterns of NWS based on the observations and all multi-model ensemble (AMME) are shown in Figure 2. Generally, in all seasonal and annual patterns, the highest observed NWS values are found in northern, northeastern, and northwestern China, with maximum values over the TP and Inner Mongolia, while the lowest NWS values are mainly localized over southern–central China, with the smallest values centered in western Xinjiang and the Sichuan Basin (Figure 2a–e). The study of Jiang et al. [14] have showed that CMIP5 (CMIP3) could reproduce the characteristics of multi-year average NWS over China with larger values in coastal and north but smaller values in inland and south regions. The spatial distributions of simulated NWS (Figure 2f–j) in CMIP6 also show patterns that are reasonably similar to those of the associated observations, i.e., low (high) NWS values in southern (northern) China. However, relative to the observations, AMME generally overestimates NWS over most of mainland China, and the most pronounced positive biases can be seen in the west portion of Xinjiang and east of the TP (Figure 2k–o). This finding is inconsistent with the results of previous studies, which indicate that CMIP5 simulations tend to overestimate the NWS over China during recent decades [14,16,17]. Furthermore, the biases are more pronounced in winter and autumn than in spring and summer. Overall, the CMIP6 GCMs are considered capable of generally reproducing the mean spatial climatological pattern of NWS over China reasonably well.

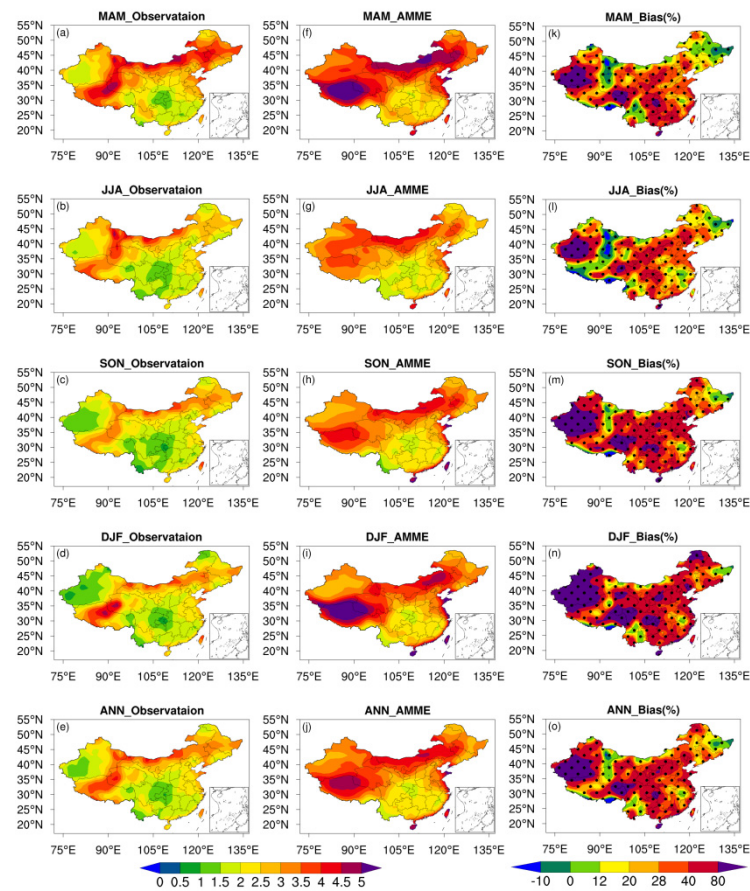


Figure 2. Spatial distributions of (a–e) observed NWS ($\text{m}\cdot\text{s}^{-1}$), (f–j) AMME simulated NWS ($\text{m}\cdot\text{s}^{-1}$), and (k–o) AMME simulation biases relative to the observations (i.e., simulation minus observation/observation) for the historical period. Black solid dots represent that the absolute bias passed the 95% significance test.

Taylor diagrams that depict the spatial correlation coefficient (SCC), normalized standard deviation (STD), and centered RMSE (CRMSE) of the climatological annual and seasonal NWS over China simulated by each of the CMIP6 GCMs and AMME against the observations for the period 1975–2014 are presented in Figure 3. Wu et al. [27] have pointed out that the multi-model ensemble of CMIP6 generally performs better in simulating the spatial distribution of NWS over China than CMIP5. In our paper, it can be seen that the SCC of each models varies in the range of 0.38–0.82, except that of INM-CM4-8 and INM-CM5-0 in summer, indicating that most simulated fields of annual and seasonal NWS match well with those based on the observations. The STD (CRMSE) values are generally 0.71–1.91 (0.73–1.63) for the annual mean, 0.64–1.85 (0.64–1.60) in spring, 0.73–1.93 (0.71–1.56) in summer, 0.73–2.14 (0.79–1.86) in autumn, and 0.77–2.39 (0.82–2.13) in winter. However, the STD (CRMSE) values of MRI-ESM2-0 are much poorer, that is, 2.77, 2.38, 2.81, 2.87, and 2.81 (2.42, 2.05, 2.36, 2.60, and 2.51) for the annual mean, spring, summer, autumn, and winter respectively, illustrating that this certain model have limited capability in capturing the spatial variability of NWS climatology over China. From above analysis, the annual and seasonal SCCs, normalized standard deviations, and CRMSEs are in the ranges of 0.12–0.82, 0.64–2.87, and 0.64–2.88, respectively.

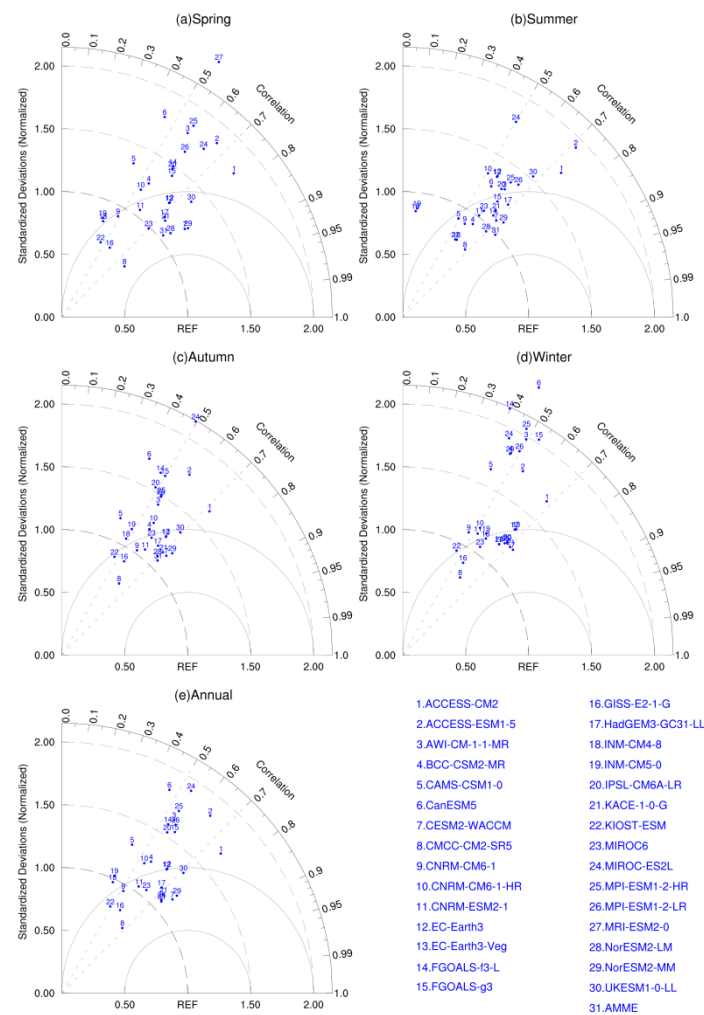


Figure 3. Taylor diagrams of (a) spring, (b) summer, (c) autumn, (d) winter, and (e) the annual mean for CMIP6 simulations in comparison with observations over China during 1975–2014. In the Taylor diagrams, angular axes show the spatial correlation coefficient (SCC) between the simulations and observations, radial axes show the spatial standard deviation (STD) normalized against that of the observations, and dashed arcs show the centered root mean square error (CRMSE). Numbers 1–31 represent the different CMIP6 models and AMME, and “REF” represents the observed NWS, which is at the intersection of the SCC of 1 and STD of 1. The closer the position is to REF, the better the performance of the model when not considering relative bias.

In the contrast between different seasons, the CMIP6 models perform well in simulating the spatial pattern of NWS in summer and autumn, followed in descending order by winter, spring, and the annual mean. The models with better performance in simulating NWS maintain that performance in all seasons and in terms of the annual mean. Overall, the CRMSEs of the CMCC-CM2-SR5, CESM2-WACCM, NorESM2-LM, NorESM2-MM, KACE-1-0-G, GISS-E2-1-G, HadGEM3-GC31-LL, and MIROC6 models are <1 in all seasons and in terms of the annual mean, indicating that these models have reasonable capability in reproducing the spatial pattern of NWS over China.

Better simulation capability means that a model is not only able to effectively reproduce the spatial pattern of the climatology of NWS but also has small deviation. The nationally averaged seasonal and annual relative biases of each CMIP6 model are shown in Figure 4. Previous study on CMIP3 showed that the simulated mean NWS over China of most models is less than observations [28], while CMIP5 overestimates the NWS over China [29]. It can be clearly seen from the figure that most models of CMIP6 tend to overestimate NWS on both seasonal and annual time scales, and the surface parameterization

process used in GCMs may be the main factor causing the overestimation of NWS [29]. The bias is largest in winter, it is smaller on the annual time scale and in autumn, and smallest in spring and summer. This may be related to the overestimation of most CMIP6 models in all seasons, whereas the observations of NWS over China are largest in spring. Except for the AMME, which shows a small deviation, the CMCC-CM2-SR5, MIROC6, HadGEM3-GC31-LL, UKESM1-0-LL, KACE-1-0-G, and ACCESS-CM2 models show smaller bias (with an absolute value of relative deviation of <0.2) in all seasons and on the annual basis than that of the other models, while the CanESM5, MIROC-ES2L, BCC-CSM2-MR, MRI-ESM2-0, FGOALS-f3-L, and FGOALS-g3 models all show poor performance. Compared to another study [27] on NWS in CMIP6 over China, which showing the BCC-CSM2-MR, CAMS-CSM1-0, CanESM5, FGOALS-f2-L, and MRI-ESM2-0 models performed well in spatial characteristic simulation, the results of the case study and composite-based analysis in our study indicate that the CMCC-CM2-SR5, KACE-1-0-G, HadGEM3-GC31-LL, and MIROC6 models can effectively reproduce the spatial distribution of NWS on both seasonal and annual time scales.

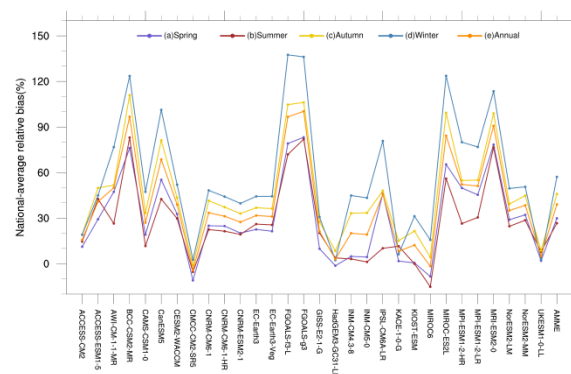


Figure 4. Nationally averaged seasonal and annual relative bias of the CMIP6 models.

3.2. Interannual Variability

In addition to the spatial distribution, temporal variation is another fundamental factor for validation of model skill. In this study, the *IVS* values were calculated for each grid box of China, and then the final statistical value was derived as the national average of all the grid box values. As mentioned in Section 2.2, as the *IVS* becomes closer to 0, the simulation capability of the model improves. The *IVS* values of each model for the interannual variability of NWS in China for each season and annually are illustrated in Figure 5. Previous studies on CMIP5 (CMIP3) showed that the models can reproduce the weakening trend of NWS over China, but the simulations significantly underestimate the magnitude of the measured trend [14,16,28,29]. It can be seen that the seasonal *IVS* values are <10 for all models except INM-CM5-0 and INM-CM4-8, which have values of 13.7 and 14.8 respectively. This indicates that the climate models are capable of reasonable reproduction of the interannual variation of seasonal NWS in China. However, large inconsistencies are found between the models and poor simulations of the interannual variability of annual NWS. The annual *IVS* is in the range of 1.4–23.8 and 12 models have values >10 , clearly larger than for the individual seasons, indicating that the CMIP6 models have poor simulation capability regarding annual NWS. Zha et al. [17] have pointed out that ACCESS1.0, CMCC-CMS, CSIRO-MK3.6.0, HadCM3, and HadGEM2-ES models in CMIP5 have the better performance on interannual variability of NWS in eastern China. While for CMIP6, the MIROC-ES2L, FGOALS-f3, BCC-CSM2-MR, and MPI-ESM1-2-HR models exhibit the best performance in terms of the temporal variation over China on both seasonal and annual time scales, whereas the INM-CM5-0, CMCC-CM2-SR5, and INM-CM4-8 models demonstrate the poorest capability in reproducing the interannual variability of NWS.

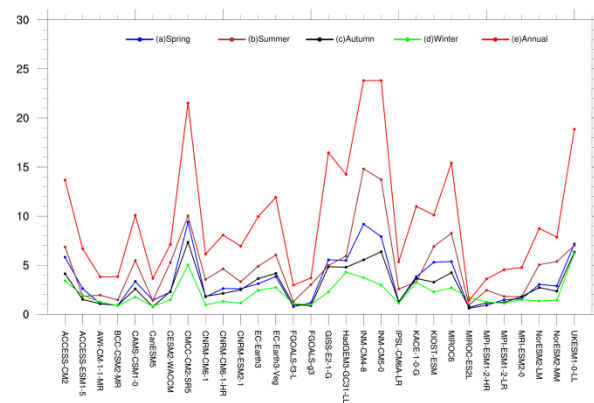


Figure 5. Interannual variability score (*IVS*) of the CMIP6 models in terms of seasonal and annual NWS over China.

3.3. Optimal Models

To compare the overall performance of the CMIP6 models, a heatmap of seasonal and annual NWS based on consideration of the Taylor diagrams, *BIAS*, and *IVS* is presented in Figure 6a. It is clear from the figure that most models do not have sufficient capability to reproduce both the spatial pattern and interannual variability well. Therefore, to identify those models with the best performance in simulating both the spatial distribution and the interannual variability of NWS, the *MR* value of each of the 30 models was calculated using Equation (8). As can be seen from Figure 6b, the KIOST-ESM, CNRM-ESM2-1, HadGEM3-GC31-LL, CMCC-CM2-SR5, and KACE-1-0-G models are ranked as the top five best-performing models (*MR* values of >0.6) in simulating NWS over China, whereas the MRI-ESM2-0, MIROC-ES2L, ACCESS-ESM1-5, FGOALS-g3, and CanESM5 models are the five poorest-performing models (*MR* values of <0.4).

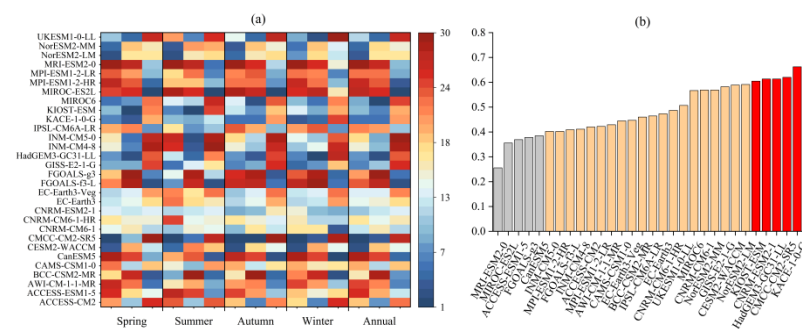


Figure 6. (a) Heatmap of the ranking of the performance of the CMIP6 models in reproducing the seasonal and annual NWS in China ($m \cdot s^{-1}$). The grid boxes from left to right present the ranking of the Taylor diagram, *BIAS*, and *IVS*, respectively. (b) Histogram of the *MR* for each model based on the Taylor diagrams, *BIAS*, and *IVS*.

Taking the annual NWS as an example, Figure 7 shows the spatial distribution of the absolute deviation and temporal correlation between the observations and the CMIP6 simulations of AMME, the best multi-model ensemble (BMME), and the poorest multi-model ensemble (PMME). In terms of absolute deviation in Figure 7a–c, although all the results of AMME, BMME, and PMME show considerable overestimation over western and northern China, especially in the Tarim Basin, it is evident that BMME has the smallest deviation over most regions of China. In terms of temporal correlation in Figure 7d–f, it is shown that AMME can simulate the temporal variation well over most parts of western China but fails to reproduce the positive correlation over eastern China. Similarly, PMME cannot accurately simulate the temporal variation in most regions of China, especially in southwestern, central, and northeastern parts. For BMME, the positive correlation

coefficient is maintained over most of China, except northeastern and southwestern regions. Therefore, BMME is reasonably capable of reflecting the spatial distribution and temporal variation of observed NWS over recent decades.

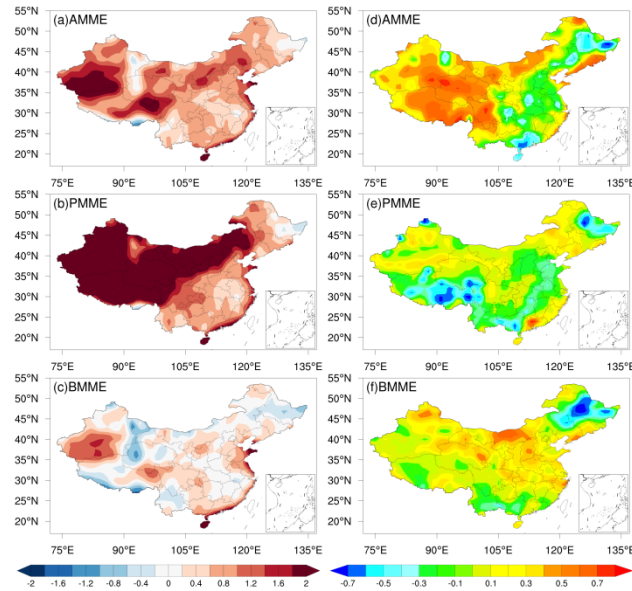


Figure 7. Spatial distribution of (a–c) absolute bias ($m \cdot s^{-1}$) and (d–f) temporal correlation for AMME, PMME, and BMME between the observations and CMIP6 simulations of annual NWS over China.

4. Future Projections Based on Optimal Multi-Model Ensemble

4.1. Temporal Evolution

On the basis of the five best-performing models, the climatological monthly distributions of NWS during the historical period and under different future scenarios are shown in Figure 8. It is apparent from the figure that the monthly distribution of NWS under each of the different scenarios is consistent with that of the historical period, demonstrating the characteristics of “one peak and one valley”; that is, MAM is the season of strong wind and JAS is the season of weak wind. Furthermore, the future NWS over China in all months under each of the different scenarios is weaker than in the historical period, with the largest deviation in April–June and September–November. Notably, the weakening of NWS under SSP5-8.5 is smaller than that under SSP1-2.6 in winter, spring, and summer, but larger in autumn; moreover, it is also larger than that under SSP2-4.5 in most months.

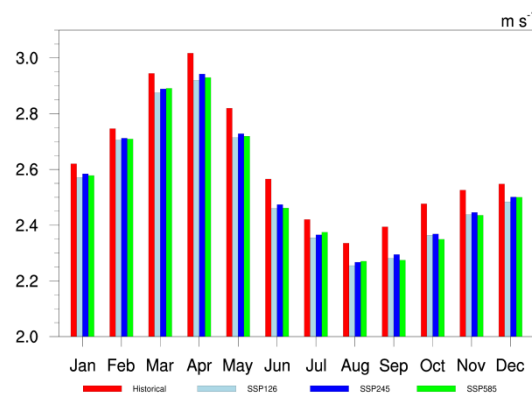


Figure 8. Climatological monthly distribution of NWS over China in the historical period and under different future scenarios.

The nationally averaged time series of summer, winter, and annual NWS over China under the different future scenarios are illustrated in Figure 9. It is obvious that the

interannual variability of projected NWS over China of CMIP6 is consistent with previous studies on CMIP3 [15] and CMIP5 [29], which all showed a modest trend in the future. For the annual series, the NWS (Figure 9a) varies in the range of 2.49–2.59 $\text{m}\cdot\text{s}^{-1}$ and all series present considerable interannual variability with significant weakening trends of -0.005 , -0.003 , and $-0.007 \text{ m}\cdot\text{s}^{-1}\cdot 10\text{a}^{-1}$ for SSP1-2.6, SSP2-4.5, and SSP5-8.5, respectively. The weakening trend of NWS is the largest under the SSP5-8.5 scenario, consistent with the findings of Karnauskas et al. [2] in mid-latitude and Zha et al. [17] in eastern China. For seasonal NWS (Figure 9b,c), the series varies in the range of 2.31–2.42 $\text{m}\cdot\text{s}^{-1}$ in summer and 2.51–2.69 $\text{m}\cdot\text{s}^{-1}$ in winter. The seasonal NWS is also projected to weaken during the 21st century, except under the SSP2-4.5 scenario in winter, which is associated with the offset of positive and negative trends of NWS in different grid regions over China under this scenario (Figure omitted). Where the trends of summer are -0.005 , -0.003 , and $-0.004 \text{ m}\cdot\text{s}^{-1}\cdot 10\text{a}^{-1}$ under SSP1-2.6, SSP2-4.5, and SSP5-8.5, respectively, and -0.003 , and $-0.005 \text{ m}\cdot\text{s}^{-1}\cdot 10\text{a}^{-1}$ in winter for SSP5-8.5 and SSP1-2.6, respectively.

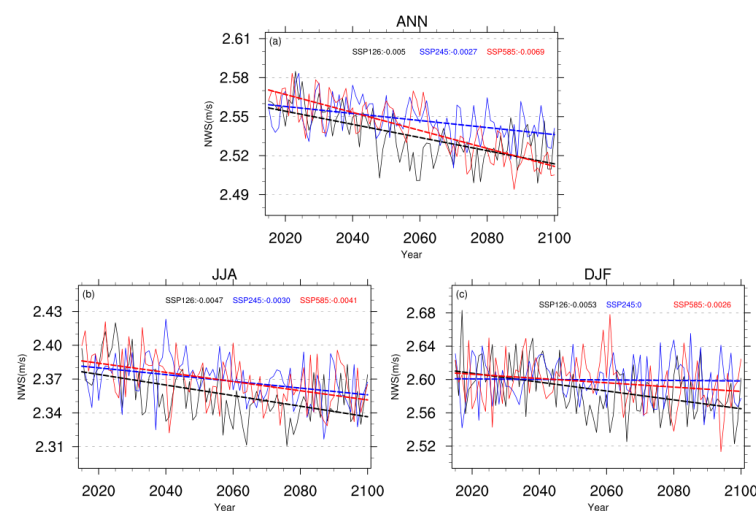


Figure 9. Time series of nationally averaged (a) annual, (b) summer, and (c) winter NWS over China under SSP1-2.6 (black line), SSP2-4.5 (blue line), and SSP5-8.5 (red line), with the trends passing the 99% statistical significance test.

4.2. Spatial Patterns

The projected spatial changes of NWS for the early period (2021–2060) and later period (2061–2100) of the 21st century relative to the reference period (1975–2014) under the three future scenarios are displayed in Figures 10 and 11, respectively. In the early period (Figure 10), the spatial distributions of annual NWS under the three scenarios are reasonably similar over most of China (Figure 10a,d,g). For example, the projected NWS over most parts of China is weaker than in the historical period, where the TP has the largest negative center (below $-0.15 \text{ m}\cdot\text{s}^{-1}$). The study of Jiang et al. [15] and Chen et al. [29] also found that the future NWS on TP will reduce by the largest amount over China in CMIP5. Whereas positive values are located over different regions under the different scenarios, and this scattered distribution of positive changing regions in the future was also found in a previous study [27]. For summer and winter NWS, the TP is also the region with large negative values but with a smaller (larger) area in summer (winter), and the regions with positive values are located mainly in southern (northern) China in summer (winter), which is similar to the seasonal spatial features based on multi-model ensemble of CMIP5 estimation [15]. In the later period (Figure 11), the spatial patterns of projected changes of NWS over China are largely similar to those of the early period for all future scenarios, but the area of the regions with obvious weakening is expanded much more than in the early period over the TP and northeastern China. And generally,

the magnitude of the weakening of NWS over the TP is larger and the area with positive bias is wider owing to the strengthening of radiative forcing.

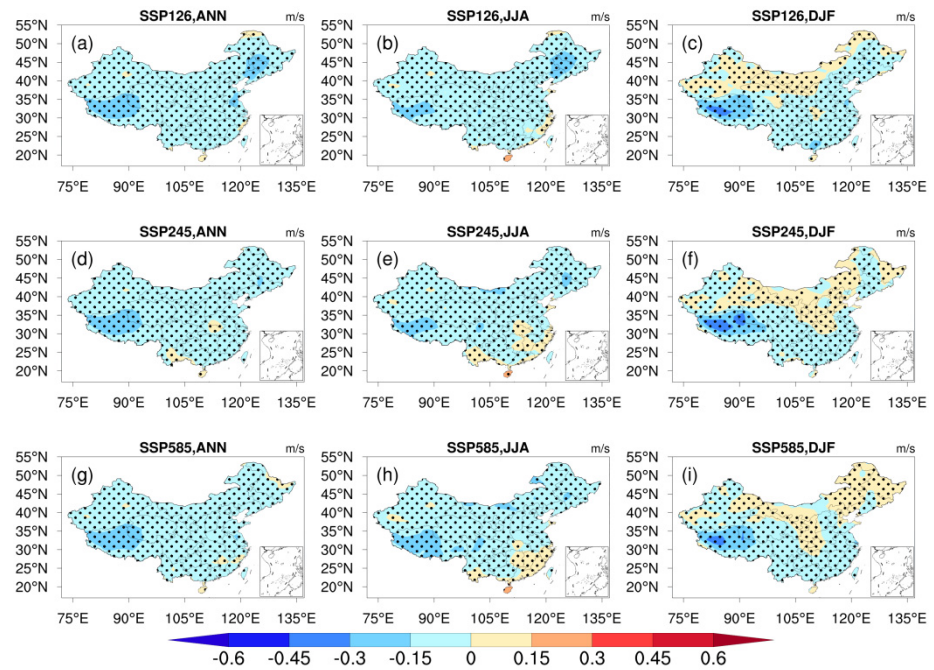


Figure 10. Projected changes of NWS ($\text{m}\cdot\text{s}^{-1}$) under (a–c) SSP1-2.6, (d–f) SSP2-4.5, and (g–i) SSP5-8.5 for the period 2021–2060 relative to the reference period (1975–2014). The first column (a,d,g) is annual, the second column (b,e,h) is summer, and the third column (c,f,i) is winter variation. Black solid dots indicate those grids with statistically significant changes at the 95% level.

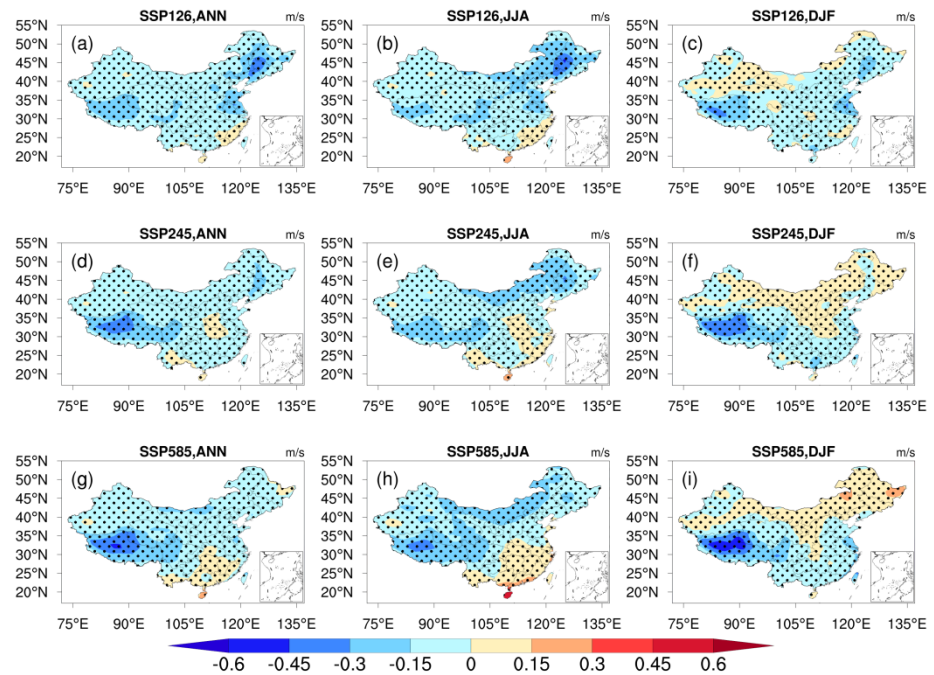


Figure 11. Same as Figure 10, but for the later period (2061–2100).

5. Discussion and Conclusions

This study evaluated the performance of 30 CMIP6 GCMs in simulating NWS over China, and investigated the projected future changes of NWS under three emission scenarios (SSP1-2.6, SSP2-4.5, and SSP5-8.5) based on an optimal multi-model ensemble. The main conclusions are as follows:

(1) Most of the CMIP6 models could reproduce the spatial patterns of seasonal and annual NWS well, although the models generally overestimated NWS at both seasonal and annual time scales and the bias was large (small) in winter (spring and summer).

(2) All the models tended to underestimate the temporal variability of seasonal and annual NWS; however, they were better able to reproduce the interannual variability of NWS in winter than that in autumn, spring, and summer and on the annual time scale. Only the MIROC-ES2L, FGOALS-f3-L, BCC-CSM2-MR, and MPI-ESM1-2-HR models could simulate the interannual variability of seasonal and annual NWS well.

(3) The KIOST-ESM, CNRM-ESM2-1, HadGEM3-GC31-LL, CMCC-CM2-SR5, and KACE-1-0-G models ranked as the five best-performing models according to a comprehensive ranking index. In comparison with AMME and PMME, BMME was better able to reflect the changes of the observations.

(4) In the future, NWS in all months under the different scenarios is projected to be weaker than in the historical period, and NWS in most regions of China will weaken under all future scenarios, especially over the TP. The nationally averaged annual mean NWS presented considerable interannual variability with significant trends of weakening of -0.005 , -0.003 , and $-0.007 \text{ m}\cdot\text{s}^{-1}\cdot 10 \text{ a}^{-1}$ for SSP1-2.6, SSP2-4.5, and SSP5-8.5 respectively, and the seasonal NWS is also projected to weaken during the 21st century, except under the SSP2-4.5 scenario in winter.

Since most of China is located in mid-latitude with an obvious monsoon climate, we mainly focused on the impact of high–low-latitude gradient and monsoon on NWS. We depicted (Figure omitted) the change of surface temperature and the zonal mean of surface temperature in northeast hemisphere ($30\text{--}180^\circ \text{ E}$, $0\text{--}90^\circ \text{ N}$), and we also calculated the index of East Asian summer monsoon (EASM) and East Asian winter monsoon (EAWM) under future scenarios according to the definitions in [30,31], respectively. We found that the general decrease of NWS is related to the decrease of the meridional temperature gradient caused by the “polar amplification effect” of global warming, which leads to a decrease of temperature gradient at mid-latitudes, and to further weakening the intensity and frequency of storm tracks [2]. The different change that the regions with positive values face, located mainly in southern (northern) China in summer (winter), is related to the intensity of monsoon under future scenarios. In our study, the increasing trends of the EASM blowing inland from the ocean and the EAWM blowing the ocean from inland have an important influence on the future NWS in summer (winter).

Our study provides a reference for model improvement and related scientific research, and it is also important with regard to future wind power development and policy formulation for sustainable development. However, uncertainty remains in the prediction of future NWS by climate models. Therefore, it would be worthwhile to conduct further research on optimization of model frameworks and improvement of multi-model integration methods. Furthermore, many factors affect the change of NWS, and the linkages between these related factors are complex. The analysis of the possible effects of other factors on changes of NWS under different future scenarios is worthy of further investigation.

Author Contributions: Conceptualization, W.H. and G.F.; Data curation, H.D.; Formal analysis, W.H., H.D. and G.F.; Methodology, H.D.; Project administration, W.H.; Resources, W.H.; Software, H.D.; Validation, H.D.; Visualization, H.D.; Writing—original draft, H.D.; Writing—review and editing, W.H. and G.F. All authors have read and agreed to the published version of the manuscript.

Funding: This research was funded by the National Natural Science Foundation of China (41775072, 42075019), the Chinese National Key R&D Program of China (2018YFC1505702), the second Ti-

betan Plateau Scientific Expedition and Research Program (2019QZKK010203), and the Science and Technology Program of Sichuan province (2019JDJQ0001).

Institutional Review Board Statement: Not applicable.

Informed Consent Statement: Not applicable.

Data Availability Statement: The CMIP6 model data and station data used in this work are available from World Climate Research Programme Coupled Model Intercomparison Project (<https://esgf-node.llnl.gov/projects/cmip6/>, accessed on 11 August 2021) and China Meteorological Data Service Centre (<http://data.cma.cn/>, accessed on 11 August 2021), respectively.

Acknowledgments: The authors would like to acknowledge the detailed comments and suggestions from three anonymous reviewers.

Conflicts of Interest: The authors declare no conflict of interest.

References

1. WWEA. Worldwide Wind Capacity Reaches 744 Gigawatts—An Unprecedented 93 Gigawatts Added in 2020. Available online: <https://wwindea.org/worldwide-wind-capacity-reaches-744-gigawatts/> (accessed on 10 July 2021).
2. Karnauskas, K.B.; Lundquist, J.K.; Zhang, L. Southward shift of the global wind energy resource under high carbon dioxide emissions. *Nat. Geosci.* **2018**, *11*, 38–43. [[CrossRef](#)]
3. Solaun, K.; Cerdá, E. Impacts of climate change on wind energy power—Four wind farms in Spain. *Renew. Energ.* **2020**, *145*, 1306–1316. [[CrossRef](#)]
4. Pryor, S.C.; Barthelmie, R.J. Climate change impacts on wind energy: A review. *Renew. Sustain. Energy Rev.* **2010**, *14*, 430–437. [[CrossRef](#)]
5. Xu, C.; Guan, Q.; Lin, J.; Luo, H.; Yang, L.; Tan, Z.; Wang, Q.; Wang, N.; Tian, J. Spatiotemporal variations and driving factors of dust storm events in northern China based on high-temporal-resolution analysis of meteorological data (1960–2007). *Environ. Pollut.* **2020**, *260*, 114084. [[CrossRef](#)]
6. Zeng, Q.; Chen, Z.A. Review of the Effect of Meteorological Disasters on Wind Farms in Recent Years. *Adv. Meteor. Sci. Technol.* **2019**, *9*, 49–55. (In Chinese)
7. Wang, Z.; Ding, Y.; He, J.; Yu, J. An updating analysis of the climate change in China in recent 50 years. *Acta Meteor. Sin.* **2004**, *62*, 228–236. (In Chinese)
8. Niu, F.; Li, Z.; Li, C.; Lee, K.H.; Wang, M. Increase of wintertime fog in China: Potential impacts of weakening of the Eastern Asian monsoon circulation and increasing aerosol loading. *J. Geophys. Res. Atmos.* **2010**, *115*. [[CrossRef](#)]
9. Guo, H.; Xu, M.; Hu, Q. Changes in near-surface wind speed in China: 1969–2005. *Int. J. Climatol.* **2011**, *31*, 349–358. [[CrossRef](#)]
10. You, Q.; Fraedrich, K.; Min, J.; Kang, S.; Zhu, X.; Pepin, N.; Ling, Z. Observed surface wind speed in the Tibetan Plateau since 1980 and its physical causes. *Int. J. Climatol.* **2014**, *34*, 1873–1882. [[CrossRef](#)]
11. Wu, J.; Zha, J.; Zhao, D. Estimating the impact of the changes in land use and cover on the surface wind speed over the East China Plain during the period 1980–2011. *Clim. Dynam.* **2016**, *46*, 847–863. [[CrossRef](#)]
12. Rahim, M.; Yoshino, J.; Doi, Y.; Yasuda, T. Effects of global warming on the average wind speed field in central Japan. *J. Sustain. Energy Environ.* **2012**, *3*, 165–171.
13. Mohan, S.; Bhaskaran, P.K. Evaluation of CMIP5 climate model projections for surface wind speed over the Indian Ocean region. *Clim. Dynam.* **2019**, *53*, 5415–5435. [[CrossRef](#)]
14. Jiang, Y.; Xu, X.; Liu, H.; Dong, X.; Wang, W.; Jia, G. The underestimated magnitude and decline trend in near-surface wind over China. *Atmos. Sci. Lett.* **2017**, *18*, 475–483. [[CrossRef](#)]
15. Jiang, Y.; Xu, X.Y.; Liu, H.W.; Wang, W.B.; Dong, X.G. Projection of surface wind by CMIP5 and CMIP3 in China in the 21st century. *J. Meteorol. Environ.* **2018**, *34*, 56–63. (In Chinese)
16. Abolude, A.T.; Zhou, W.; Akinsanola, A.A. Evaluation and projections of wind power resources over China for the energy industry using CMIP5 models. *Energies* **2020**, *13*, 2417. [[CrossRef](#)]
17. Zha, J.; Wu, J.; Zhao, D.; Fan, W. Future projections of the near-surface wind speed over eastern China based on CMIP5 datasets. *Clim. Dynam.* **2020**, *54*, 2361–2385. [[CrossRef](#)]
18. Eyring, V.; Bony, S.; Meehl, G.A.; Senior, C.A.; Bjorn, S.; Stouffer, R.J.; Taylor, K.E. Overview of the Coupled Model Intercomparison Project Phase 6 (CMIP6) experimental design and organization. *Geosci. Model. Dev.* **2016**, *9*, 1937–1958. [[CrossRef](#)]
19. O’Neill, B.C.; Tebaldi, C.; Vuuren, D.P.; Eyring, V.; Friedlingstein, P.; Hurtt, G.; Knutti, R.; Kriegler, E.; Lamarque, J.F.; Lowe, J.; et al. The scenario model intercomparison project (ScenarioMIP) for CMIP6. *Geosci. Model. Dev.* **2016**, *9*, 3461–3482. [[CrossRef](#)]
20. Li, S.; Miao, L.; Jiang, Z.; Wang, G.; Gnyawali, K.; Zhang, J.; Zhang, H.; Fang, K.; He, Y.; Li, C. Projected drought conditions in Northwest China with CMIP6 models under combined SSPs and RCPs for 2015–2099. *Adv. Clim. Chang. Res.* **2020**, *11*, 210–217. [[CrossRef](#)]
21. Xin, X.; Wu, T.; Zhang, J.; Yao, J.; Fang, Y. Comparison of CMIP6 and CMIP5 simulations of precipitation in China and the East Asian summer monsoon. *Int. J. Climatol.* **2020**, *40*, 6423–6440. [[CrossRef](#)]
22. Yang, X.; Zhou, B.; Xu, Y.; Han, Z. CMIP6 Evaluation and Projection of Temperature and Precipitation over China. *Adv. Atmos. Sci.* **2021**, *38*, 817–830. [[CrossRef](#)]

23. Taylor, K.E. Summarizing multiple aspects of model performance in a single diagram. *J. Geophys. Res. Atmos.* **2001**, *106*, 7183–7192. [[CrossRef](#)]
24. Chen, W.; Jiang, Z.; Li, L. Probabilistic projections of climate change over China under the SRES A1B scenario using 28 AOGCMs. *J. Clim.* **2011**, *24*, 4741–4756. [[CrossRef](#)]
25. Santer, B.D.; Taylor, K.E.; Gleckler, P.J.; Bonfils, C.; Barnett, T.P.; Pierce, D.W.; TWigley, M.L.; Mears, C.; Wentz, F.J.; Brüggemann, W.; et al. Incorporating model quality information in climate change detection and attribution studies. *Proc. Natl. Acad. Sci. USA* **2009**, *106*, 14778–14783. [[CrossRef](#)]
26. Jiang, Z.; Li, W.; Xu, J.; Li, L. Extreme precipitation indices over China in CMIP5 models. *Part I Model evaluation. J. Clim.* **2015**, *28*, 8603–8619.
27. Wu, J.; Shi, Y.; Xu, Y. Evaluation and Projection of Surface Wind Speed Over China Based on CMIP6 GCMs. *J. Geophys. Res. Atmos.* **2020**, *125*. [[CrossRef](#)]
28. Jiang, Y.; Luo, Y.; Zhao, Z. Evaluation of wind speeds in China as simulated by global climate models. *Acta Meteor. Sin.* **2009**, *67*, 1020–1029.
29. Chen, L.; Pryor, S.C.; Li, D. Assessing the performance of Intergovernmental Panel on Climate Change AR5 climate models in simulating and projecting wind speeds over China. *J. Geophys. Res. Atmos.* **2012**, *117*. [[CrossRef](#)]
30. Zhao, P.; Zhou, Z. East Asian subtropical summer monsoon index and its relationships to rainfall. *Acta Meteor. Sin.* **2005**, *63*, 933–941. (In Chinese)
31. Huang, R.; Liu, Y.; Huang, J.; Feng, T. Characteristics and internal dynamical causes of the interdecadal variability of East Asian winter monsoon near the late 1990s. *Chin. J. Atmos. Sci.* **2014**, *38*, 627–644. (In Chinese)